Journal of Structural Geology 34 (2012) 43–53

Contents lists available at SciVerse ScienceDirect

Journal of Structural Geology

journal homepage: www.elsevier.com/locate/jsg

# Saw-tooth structures and curved veins related to folds in the south-central Pyrenees (Spain)

F. Bastida [a,*], J. Aller [a], R.J. Lisle [b], N.C. Bobillo-Ares [c], C.O. Menéndez [c]

[a] Departamento de Geología, Universidad de Oviedo, Jesús Arias de Velasco s/n, 33005 Oviedo, Spain
[b] School of Earth and Ocean Sciences, Cardiff University, Cardiff, CF10 3AT, UK
[c] Departamento de Matemáticas, Universidad de Oviedo, 33007 Oviedo, Spain

ARTICLE INFO

*Article history:*
Received 4 April 2011
Received in revised form
6 October 2011
Accepted 31 October 2011
Available online 10 November 2011

*Keywords:*
Folds
Fractures
Veins
Pyrenees

ABSTRACT

Two generation of folds ($F_1$ and $F_2$) and associated structures, developed in the Eocene turbidites of the south-central Pyrenees, are analyzed in this paper. $F_1$ folds are close, have sub-horizontal axes and southwards vergence. They have an associated cleavage $S_1$. Competent layers were folded by layer-parallel shortening, tangential longitudinal strain, some possible flexural flow and an obliquely superimposed homogeneous strain due mainly to simple shear. Flexural slip is also an important mechanism in the whole multilayer. $F_2$ folds are gentle and scarce; they fold the $S_1$ cleavage.

Among the structures associated with $F_1$ folds, there are sets of veins with curved form in the competent layers. The displacement of each vein gave rise usually to a step in the layer boundary, so that a set of veins produces a structure that is named "saw-tooth structure". The veins initiated as small faults that made flexural slip difficult and gave rise to a concentration of stress on the steps, leading to an opening of the fractures and a propagation of them along a curved path, as suggested by a simple mechanical model. This propagation agrees with finite element models developed by other authors.



## 1. Introduction

In the Eocene turbidites (Hecho Group) of the south-central Pyrenees, abundant metric folds developed during the Alpine deformation. It is observed in some areas that on their limbs, the competent layers contain a notable variety of veins with curious geometry. In many cases the veins have a curved wedge shape opening towards a bed boundary and involve a displacement that gives rise to the development of steps on this boundary, which is usually the stratigraphical base of the bed. As a consequence, an exotic structure not previously described in the geological literature often appears, which is named in this paper 'saw-tooth structure'.

The aim of this paper is to make an analysis of these folds and veins and to construct a mechanical model to explain their development. In the first part of the paper, the folds are described and the kinematical mechanisms involved in their evolution are analyzed. In order to accomplish that, in addition to observations and field data, computer simulations of folds have been used. This first part of the paper is necessary to explain the context and development of veins and saw-tooth structures, which are analyzed in the second part of the paper. In the latter, a mesoscopic and microscopic description of these structures is made and a model for their development is presented.

## 2. Geological setting

The Pyrenees is an Alpine belt that includes the boundary between the Iberian Peninsula and the rest of the European continent, following an E–W direction (Fig. 1). It can be divided into three parts: a central part (Axial Zone), with outcrops of a Paleozoic basement involved in the structure, and two thrust systems, a northern system with vergence to the north (North Pyrenean Zone) and a southern system with vergence to the south (South Pyrenean Zone). Despite this arrangement, the belt is asymmetrical, since the South Pyrenean Zone is wider than the North Pyrenean Zone, and overall a southerly vergence dominates. Alpine deformation took place between the Late Cretaceous and the Early Miocene. In the western and central parts of the South Pyrenean Zone (Jaca-Pamplona sector), a major foredeep basin developed, where syntectonic turbiditic sediments belonging to the Hecho Group were deposited during the Early-Middle Eocene. The studied structures developed in rocks of this group, and they have been analyzed along the N–S valleys that cross these western and central parts (Fig. 1).

* Corresponding author. Fax: +34 985103103.
*E-mail address:* bastida@geol.uniovi.es (F. Bastida).

0191-8141/$ – see front matter © 2011 Elsevier Ltd. All rights reserved.
doi:10.1016/j.jsg.2011.10.009

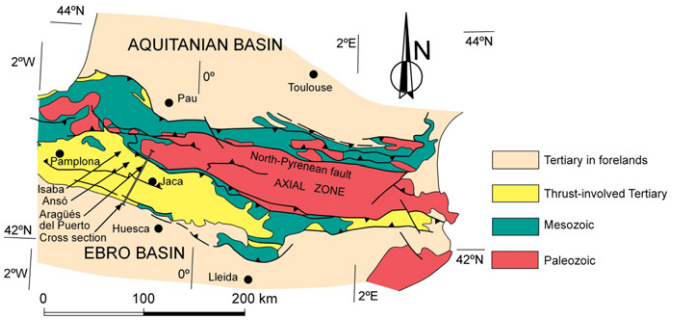


**Fig. 1.** Geological map of the Pyrenees with the location of the cross-section shown in Fig. 2 (after Mansurbeg et al., 2009). Isaba, Ansó, Aragüés del Puerto and Jaca are localities in the N–S valleys where the study folds are located.

The Hecho Group (Mutti et al., 1972) consists of a succession of arenites (hybrid arenites – sensu (Zuffa, 1980), calclithites – sensu Pettijohn et al., 1972, and siliciclastic sandstones) and shales in turbidite facies that reaches a maximum thickness of about 4500 m (Mansurbeg et al., 2009; Caja et al., 2010). The siliciclastic sandstones and the hybrid arenites contain calcite and/or dolomite cement that occludes the primary porosity.

The structure of the Jaca-Pamplona sector consists of several minor thrust systems with a basal décollement located within Triassic rocks (Gavarnie-Guarga thrust system) and a broad syncline with the trough zone in the southern part of the sector (Fig. 2). Teixell and García-Sansegundo (1995) and Teixell (1996) distinguished two generations of structures in this sector. The first consists of gently dipping thrusts with scarce associated folds and the second consists of an imbricate thrust system with numerous associated folds at mesoscopic to macroscopic scales. These folds are very common in the turbidites of the Hecho Group and have an associated cleavage in the incompetent layers. These folds and their associated veins are the main structures considered in this paper.

## 3. Analysis of folding

Observations of folds in the field permit two folding phases ($F_1$ and $F_2$) to be distinguished. $F_1$ folds are the most frequent and correspond to the second generation of regional structures; they are close folds with vergence to the southwest and an associated cleavage, $S_1$ (Fig. 3). $F_2$ folds are scarce; they are gentle folds upright or weakly vergent towards the NNE, and they fold the $S_1$ cleavage (Fig. 4). The main features of $F_1$ folds are described below.

$F_1$ folds have axes sub-horizontal or gently plunging towards the southeast or the northwest (Fig. 5a). Their axial surfaces are steeply or moderately dipping towards the NNE (Fig. 5b). Most of them are close folds (Fig. 5c). In most cases the aspect ratio (height/width ratio of the fold limb between the hinge and inflection points taking the tangent to the hinge point as horizontal) is lower than 3 and the folds mainly range in shape from chevron to parabolic (Fig. 6a), though fractures and the disorganised character of the beds prevent classification in some cases. Hence, the chevron shape is more frequent in the outcrops than it is reflected in Fig. 6a. The geometry of the competent folded beds is shown by the $s_1$–$s_2$ diagram of Bastida et al. (2005) of Fig. 6b; there is a great dispersion of points, although class 1C folds are dominant.

An $S_1$ cleavage, associated with $F_1$ folds, is well developed in the incompetent layers, mainly when the incompetent/competent thickness ratio is high. In most cases the cleavage shows divergent fanning, mainly in the hinge area (Fig. 7); nevertheless, in cases in which the incompetent beds are dominant, the cleavage tends to be parallel to the axial plane. In the competent layers, the cleavage is not developed or appears as a widely spaced convergent cleavage (Fig. 7), in which many cleavage surfaces have the appearance of fractures.

Folds approximating to chevron style have typical accommodation structures described by Ramsay (1974), such as bulbous hinges (Fig. 8a) and reverse limb faults, both associated with anomalously thick competent layers, and dilation spaces in the hinge zones with hinge collapse (Fig. 8) or flow of incompetent material towards them. Some remarkable structures have been observed on some limbs of $F_1$ folds. These are mainly curved wedge-shaped carbonate veins in competent folded beds; they are described below.

Structures associated with folding by tangential longitudinal strain are frequent, such as wedge-shaped extension fractures opening towards the outer arc in the hinge zone of competent beds (Fig. 9). These fractures are usually filled with carbonate minerals and represent a brittle expression of the tangential longitudinal strain with area change (PTLS of Bobillo-Ares et al., 2006). Exceptionally, concentric extension veins can be observed close to the inner arc of the hinge zone of the competent folded layers, also indicating tangential longitudinal strain (Fig. 7b).

Syntectonic carbonate fibres along $S_0$ can be observed in many cases in the competent–incompetent interface or inside the incompetent material. They have been found preferentially on the reverse limbs and their direction always makes an angle greater than 75° with the axial direction (Fig. 10). When fibre steps can be seen, they indicate a slip sense in agreement with the flexural slip folding mechanism, which can be associated with the tangential longitudinal strain of the competent layers.

The folds of the competent layers have a slight layer thickening in the hinge zone. Ramsay's classification of a fold in the Roncal valley made by Gil et al. (2006) suggests a flattening value ($\sqrt{\lambda_2/\lambda_1}$) between 0.7 and 0.85. However, the asymmetry between the two limbs requires an obliquity of the axes of the superimposed strain ellipse with respect to the axial plane and some heterogeneity in the flattening. This heterogeneity is also suggested by the dispersion of points in the $s_1$–$s_2$ diagram (Fig. 6b).

A folded competent layer with an axial plane dipping 57° southwards and located in the same train of folds as the fold analyzed by Gil et al. (2006) has been fitted by Aller et al. (2010) by a fold simulated by computer using the program 'Fold Modeler' (Bobillo-Ares et al., 2004) (Fig. 11). A good fit of this fold is obtained with a first folding step of isochoric layer-parallel shortening ($\sqrt{\lambda_2/\lambda_1} = 0.49$), a second step of tangential longitudinal strain without area change (ETLS of Bobillo-Ares et al., 2006) with an aspect ratio of 0.67, and a third step of flattening (pure shear with $\sqrt{\lambda_2/\lambda_1} = 0.71$) with a $\sqrt{\lambda_1}$ direction making an angle of 20° with the axial trace (angle measured clockwise facing west from the fold axial trace) (oblique flattening of Hudeleston, 1973). The considerable initial layer-parallel shortening agrees with the convergent arrangement of the cleavage present in the competent layers. The consistent direction of vergence of the folds towards the foreland and their association with thrusts with the same vergence, some of them forming duplexes at the outcrop scale near the analyzed folds (Gil et al., 2006), suggest that the folds of this area probably resulted within a rotational bulk deformation regime. Assuming a regime of simple shear strain, the strain ellipse axial ratio cited above would correspond to a foreland-directed simple shear with $\gamma = 0.35$ superimposed on a pre-existing fold and with a top-to-the-south shear sense and a direction plunging 17° north. Once the shear direction is obtained, and the $\gamma$ value and the present dip of the fold axial plane are known (Aller et al., 2010), the dip of the axial plane prior to the superimposition of the simple shear can be determined; this dip was about 66° northwards and it could be

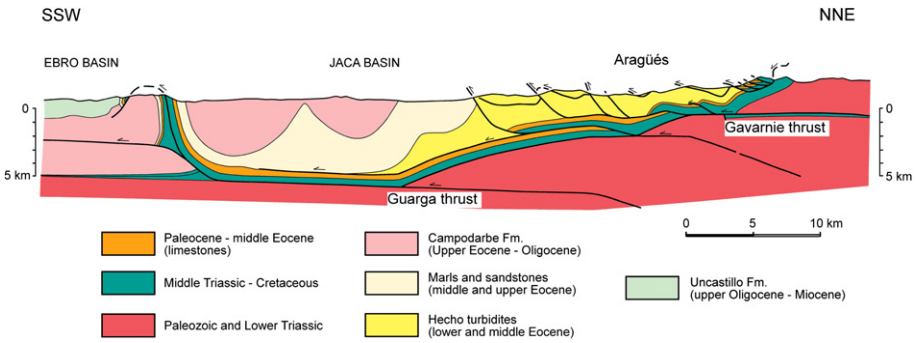


**Fig. 2.** Geological cross-section along the southern slope of the Pyrenees (after Teixell and García-Sansegundo, 1995). Location in Fig. 1.

produced, in a bulk simple shear regime, by buckling of layers oblique to the shear direction.

The competent layers of another three folds of this area have been modeled using Fold Modeler in this study. The results are similar to those obtained in the above fold, with some variations in the amount of tangential longitudinal strain without area change depending on the fold aspect ratio and minor operation of flexural flow at the end of buckling. Considering all the folds analyzed with Fold Modeler, we can infer the following kinematical evolution:

(1) A first stage of layer-parallel shortening with a $\sqrt{\lambda_2/\lambda_1}$ value between 0.49 and 0.64.
(2) A stage of tangential longitudinal strain without area change. The aspect ratio acquired by the fold by this mechanism ranges between 0.29 and 0.75.
(3) A stage of flexural flow producing an aspect ratio increment between 0 and 0.19. Thus the contribution from this mechanism is small and it does not appear in all cases.
(4) A superimposition of a small homogeneous deformation, with the major axis of the strain ellipse oblique to the axial plane. The corresponding value ranges between 0.71 and 0.96. The vergence of folds and the context of the deformation suggest that the superimposed deformation was probably non-coaxial, close to a simple shear, with a top-to-the-SSW shear sense and plunging north between 17° and 28°.

The above folds show competent layers with convergent cleavage. Nevertheless, there are many folds whose competent layers do not exhibit cleavage. These folds cannot be analyzed using Fold Modeler (Bobillo-Ares et al., 2004). The higher competence of these rocks suggests a small amount of layer-parallel shortening at the beginning of folding and operation of tangential longitudinal strain with area change, as indicated by the radial veins described above.

## 4. Veins and saw-tooth structures

Veins are very common in the rocks of the Hecho Group. They are mainly composed of carbonate minerals, chiefly dolomite. These veins often exhibit distinctive geometries that will be

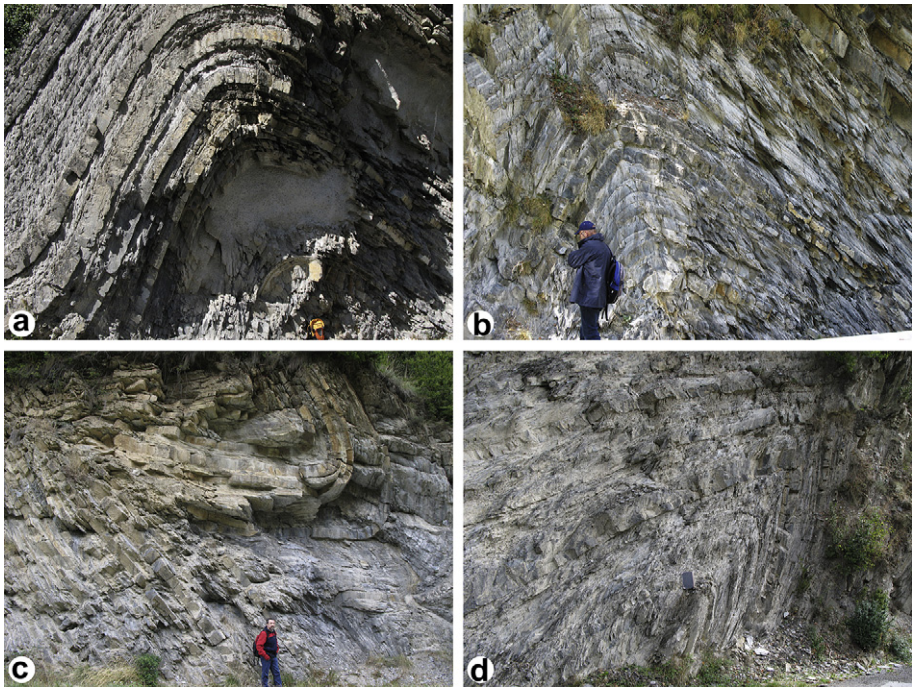


**Fig. 3.** Examples of $F_1$ folds in the study area. Note the development of cleavage $S_1$ mainly in the incompetent layers. (a), (b) and (c) South of Isaba; (d) Near Ansó. In (a), (b) and (c), north is to the right; in (d) north is to the left.

**Fig. 4.** Example of $F_2$ fold. Cleavage $S_1$ is folded. Ansó valley. North is to the left.

described below. In many cases, the development of the veins is restricted to a part of the individual competent bed, showing a wedge-like form, often curved, with a progressive thickening towards a boundary of the bed.

### 4.1. Mesoscopic description

A common pattern of veins inside a competent layer consists of two sets of wedge-shaped veins, ones opening towards the stratigraphic bottom (bottom set) and another opening towards the top (top set), with a relay disposition (Fig. 12a–f). This pattern mainly appears in the outcrops in the Aragüés del Puerto Valley (along the road from Aragüés del Puerto to the Lizara refuge, Fig. 1), and typically consists of a bottom set of curved veins combined with a top set of rectilinear or low curvature veins. They usually appear on the normal limb of the folds, although occasionally they occur on the overturned or steeper limb. On the normal limbs, the veins of the bottom set stand perpendicular to the base but bend upwards towards the north, giving rise to a concavity downwards (Fig. 12c–e). Frequently, the displacement of the vein edges gave rise to steps in the base of the bed. Their sense is such that the bedding plane steps up in the direction towards the hinge zone of the adjacent anticline. These steps mainly appear on the base and where they show a regular spacing, they form a structure that we have named 'saw-tooth structure' (Fig. 12c–e). Some bottom wedge veins show, in their mouth, pelitic material sealing the wide aperture. This appears to have formed from the adjacent rock being injected into the fracture and putting a lid on the vein. Where the top set veins are curved, the concavity has the opposite direction to that of the bottom set veins (Fig. 12f). Usually, the veins of each set terminate at the same level within the bed and the veins of the bottom set curve asymptotically towards a specific plane parallel to the layer boundaries. Hence, there is little or no overlap between the two set of veins.

A variant of the above morphology appears when the bottom set consists of veins that have a rectilinear shape. In such cases, the veins are usually oblique to bedding and cut up steeply through the bed in the direction of the adjacent syncline (Fig. 12b). In some cases, a rectilinear vein branches from a curved or angular vein (Fig. 12a, b). Exceptionally, steps associated with bottom veins coincide with steps associated with mineral fibres on the bedding plane.

Vein patterns as described above are scarce in the overturned limbs of the folds. They appear in some outcrops far from where the patterns appear in the normal limbs. In these cases, the veins are less well developed and, as in the normal limb, they are also mainly developed at the base of the bed with concavity downwards. This means that, if the beds were to be unfolded, the concavity direction of the curved bottom veins would be opposite on the two limbs.

### 4.2. Microscopic description

Four large hand specimens with veins were collected, from which 39 thin sections were made for microscopic analysis. The rocks are arenites with a mainly dolomitic cement and all samples have graded bedding. The veins consist essentially of dolomite (Fig. 13a–d). In most cases, vein boundaries are sharp, frequently cuspate or more irregular; an optical continuity of the crystals of the veins and the grains of the host rock is not observed. The shape orientation of the vein crystals is not in general very strong; there are many cases without orientation (Fig. 13c, d), cases with a weak to good orientation (Fig. 13a) and cases with parts of the vein with orientation alternating with parts without orientation (Fig. 13b).

A longitudinal discontinuity is sometimes found inside the veins. This discontinuity usually cross-cuts the crystals, although in some cases it coincides in parts with grain boundaries. The discontinuities do not produce usually a jump in the optical orientation of the crystal and they seem to be fractures in most cases.

Another characteristic feature of some veins is the existence of mudstone inside the wider end of the vein (Fig. 13c). This feature appears commonly in those veins enlarged towards the base of the bed, and more rarely in the veins enlarged towards the top. The muddy material usually shows a local foliation that is usually better developed at the margins of the vein. It seems to be the result of the flow during the mud injection. Vein-related steps can be observed

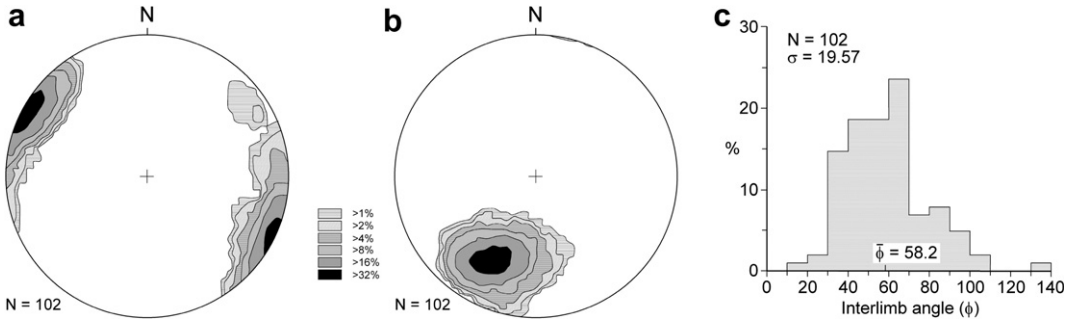


**Fig. 5.** Contoured equal-area lower hemisphere projection of the fold axes (a) and of the poles to axial surfaces (b) of $F_1$ folds. (c) Frequency diagram of the interlimb angle of $F_1$ folds. *N*, number of data; $\sigma$, standard deviation; $\bar{\phi}$, mean value.

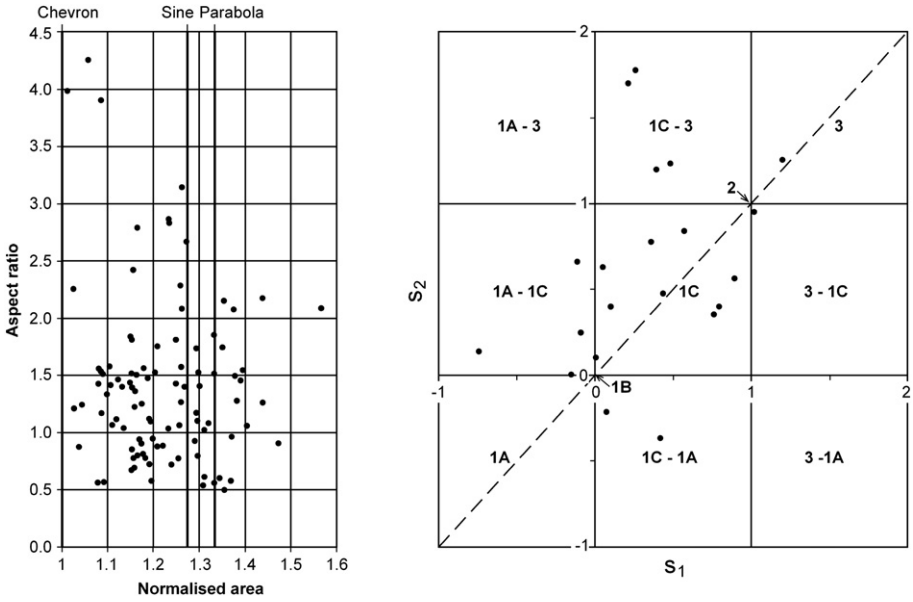


**Fig. 6.** (a) Diagram of aspect ratio vs. normalised area for $F_1$ folds. (b) Diagram of $s_1$ vs. $s_2$ for $F_1$ folded layers.

in some cases in the base of the layer (Fig. 13d). The step corner can appear rounded as a result of the deformation due to the flow of the adjacent incompetent material.

### 4.3. Origin and development of the veins and saw-tooth structures

Some features described provide evidence of the geological conditions that controlled the development of the veins and saw-tooth structures. The different development of these structures on the two limbs of the folds, the different facing-direction of the steps of the saw-tooth structures and the different facing-direction of the concavity of the bottom veins on the two limbs if they are unfolded suggest that the development of these structures is contemporaneous with the folds. Another argument supporting this interpretation is the parallelism between the vein/bedding intersection lineation and fold hinges. This geometrical relation suggests that the development of these remarkable structures was related to the stresses and strains generated during folding.

A specific factor that could favour the development of veins was the existence of a high pore pressure in the rocks during deformation, mainly in the incompetent pelitic material, where a large volume of diagenetic fluids was probably concentrated. The existence of these fluids is supported by the dolomitization processes undergone by the rocks and for the mineralizations involved in the development of the veins, which sometimes appear concentrated in swarms. High pore pressure is indicated by the pelitic material injected into the part of the veins where these meet the layer boundary (Fig. 13c). This pressure should favour a brittle behavior of the rock and the development of fractures in the competent layers.

As regards the relation between the folding mechanisms and the development of veins and saw-tooth structure, the tangential longitudinal strain and the homogeneous strain must be rejected as responsible for these exotic structures. Tangential longitudinal strain does not produce appreciable strain on limbs where the curvature of the layers is negligible, and the homogeneous strain cannot explain a brittle deformation located in bands adjacent and parallel to the layer boundaries. The fit of several folds using the computer program 'Fold Modeler' shows a limited participation of flexural flow in their development. Nevertheless, the folded competent layers fitted by 'Fold Modeler' have cleavage, whereas the layers with veins and saw-tooth structure lack an obvious cleavage. This suggests a greater competence contrast in the cases where these structures are observed and less favourable conditions for flexural flow. Therefore, the more probable mechanism to explain 'a priori' the development of vein and saw-tooth structures is flexural slip. This agrees with the existence in one outcrop of steps that are common to veins and to mineral fibres associated to flexural slip.

Any explanation of the formation of the veins and saw-tooth structure requires clarifying, in particular the origin of the steps

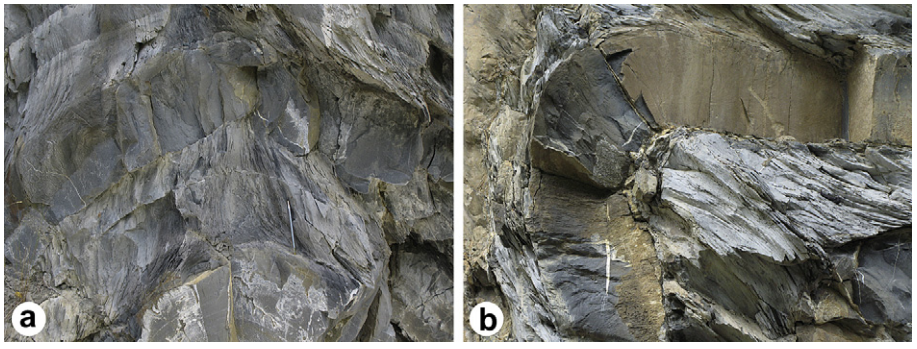


**Fig. 7.** Examples of cleavage $S_1$ showing the different fan pattern in competent and incompetent layers. South of Isaba. North to the right.

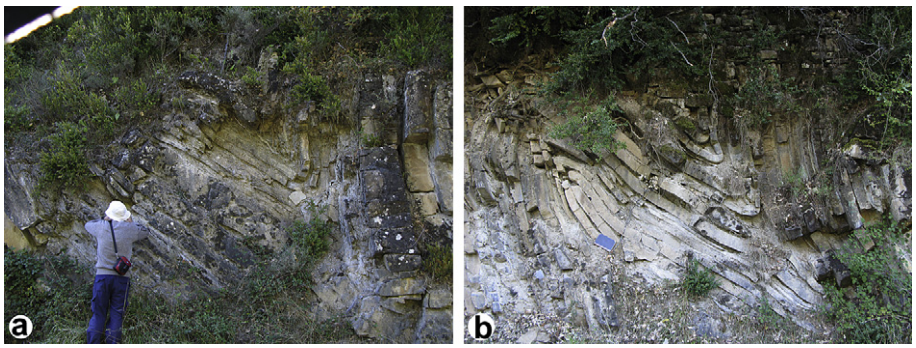


**Fig. 8.** Structures associated with chevron folds. (a) bulbous hinge; (b) hinge collapse. North of Aragües del Puerto. North to the right.

and the opening of the fracture and the development of its curvature. The steps involve a displacement tangential to the fracture surface that is characteristic of shear fractures, but on the other hand the opening associated with the veins suggests extension fractures. It is probable that the complex displacement pattern observed is the result of the formation of the veins by the operation of different fracture mechanisms during a progressive evolution. In a first stage, a significant slip along a boundary of the bed should involve a stress state with the principal directions oblique to the bedding in zones adjacent to the boundary between layers. Favoured by a high fluid pressure, this stress state could generate small faults in the competent layer near to the boundary that form a high angle with the layer boundary. These faults formed a conjugate fault set with the bedding fault involved in the mechanism of flexural slip. The existence of graded bedding in the competent layers probably favoured a better development of the fractures from the base of the bed than at the top; in fact, structural and microstructural changes in the sandstones have a notable effect on the development on fractures and veins in the study area as shown in the example of Fig. 14.

Once the steps had initiated, they could have operated as obstacles to flexural slip and this could have given rise to a stress concentration on the steps that could have contributed to the opening of the veins. In addition, the difficulty of continued flexural slip caused by the development of the faults would have favoured operation of an alternative mechanism of folding. The high competence of the layer would prevent the development of appreciable ductile strain and should favour brittle fracture. Under these conditions, the stresses inside the competent layer should give rise to a propagation of the small faults as tension gashes in agreement with the orientation of the principal stresses inside the layer, producing a curved path for the fractures. Opening of the fractures with curved trends should enable balancing of the slip loss at the end of the fault inside the layer. The character of surfaces of weakness represented by the faults enabled their propagation instead of the development of new fractures. The rock anisotropy could favour in some cases that the propagation of the gash tends asymptotically to parallelism with the bedding (Fig. 12d). In a few cases, straight veins branch obliquely from the fault indicating a spatial interference of two fractures instead of a propagation of the fault (Fig. 12a, b).

A simple 2D mechanical model produces the characteristics of the stress driving the growth and curvature of the gashes. Let us assume a layer containing several fractures initiated as small faults and separated by a distance $l$ (Fig. 15a). Let us consider the forces that operate on a rock element laterally bounded by two adjacent faults (Fig. 15b). In this figure, $\tau$ and $\tau'$ are shear stresses on the

**Fig. 9.** Hinge zone showing wedge-shaped veins opened towards the outer arc in a competent layer. Tension gashes associated with a shear zone can be seen in the lower part of the picture. South of Isaba. North to the right.

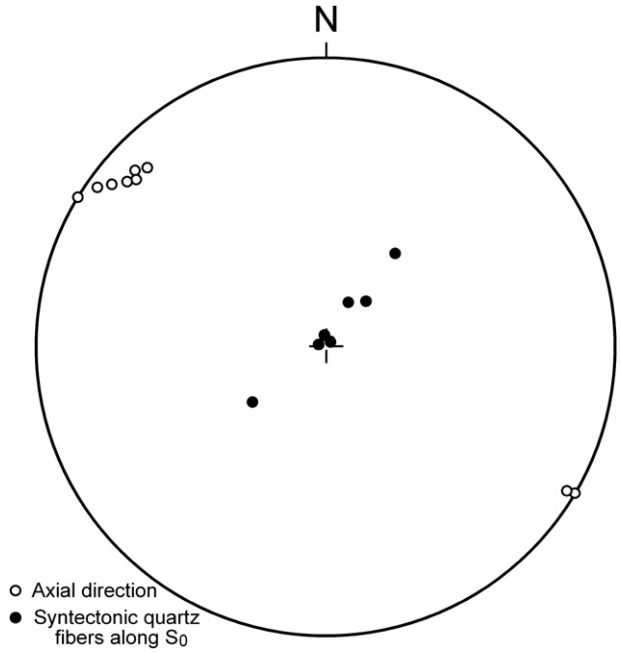


**Fig. 10.** Orientation of the syntectonic quartz fibres along $S_0$ and the corresponding fold axes. The points representative of fibres define a subvertical plane approximately perpendicular to the fold axes.

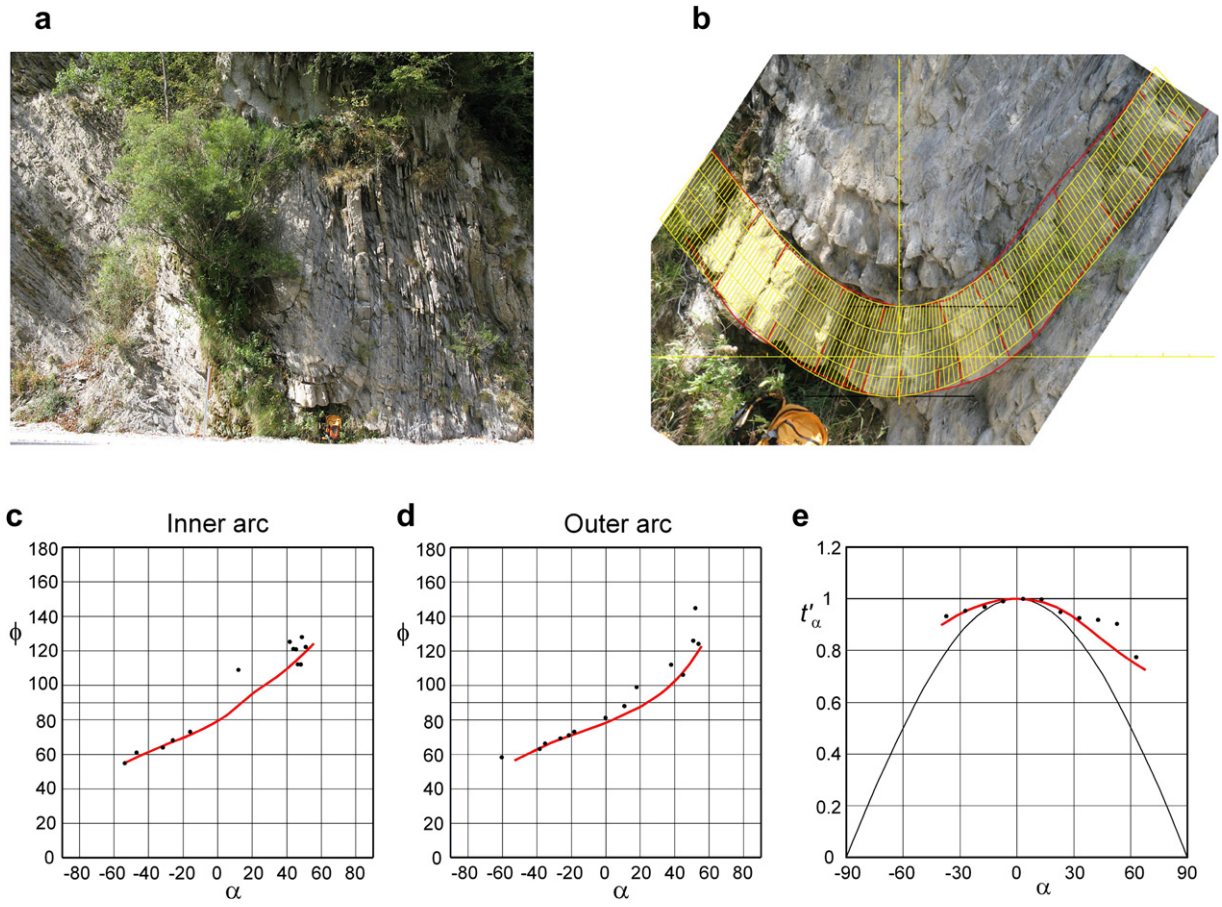


**Fig. 11.** Fit of a $F_1$ syncline (a) using 'FoldModeler' (south of Isaba; looking to the west). (b) Superimposition of the theoretical fold on the natural fold. The fold has been rotated to have its coordinate axes superposed on those of the numerical fold. Details of the modelling are given in the text. (c) and (d) Comparison of $\theta-\alpha$ curves for the numerical fold (red line) with the data of the natural fold (black points). (e) Comparison of the Ramsay's classification for the theoretical (red line) and the natural fold (black points) (after Aller et al., 2010).

lower and the upper boundaries respectively, $\sigma$ is the normal stress on the lower boundary, and $F$ is the force on the step generated previously by the a small fault (AC in Fig. 15a, b). The lateral forces operating on the wall of the fractures have not been considered nor represented in Fig. 15b, since they do not generate resulting force or moment. Under normal conditions, using the vector basis $(\hat{\mathbf{e}}_1, \hat{\mathbf{e}}_2)$ shown in Fig. 15a, the involved force vectors are $\tau\hat{\mathbf{e}}_1$, $-\tau'\hat{\mathbf{e}}_1$, $\sigma\hat{\mathbf{e}}_2$ and $F\hat{\mathbf{e}}_1$, being $\tau$, $\tau'$, $\sigma$, $F$ positive numbers. In the above basis, the stress tensor in the proximity of point C is represented by the matrix:

$$\Sigma = \begin{pmatrix} \sigma_{11} & \sigma_{12} \\ \sigma_{21} & \sigma_{22} \end{pmatrix}, \quad \sigma_{12} = \sigma_{21} \tag{1}$$

In order to determine the elements of the matrix, let us obtain the forces $\mathbf{F}^h$ and $\mathbf{F}^v$ that operate on two perpendicular surface elements at $C$ (Fig. 15c, d):

$$\mathbf{F}^h = F_1^h\hat{\mathbf{e}}_1 + F_2^h\hat{\mathbf{e}}_2 \tag{2}$$

$$\mathbf{F}^v = F_1^v\hat{\mathbf{e}}_1 + F_2^v\hat{\mathbf{e}}_2 \tag{3}$$

From the surface elements shown in Fig. 15c, d, we can write the following matrix equations:

$$\begin{pmatrix} \sigma_{11} & \sigma_{12} \\ \sigma_{21} & \sigma_{22} \end{pmatrix}\begin{pmatrix} 0 \\ -\frac{l}{2} \end{pmatrix} = \begin{pmatrix} F_1^h \\ F_2^h \end{pmatrix} \tag{4}$$

$$\begin{pmatrix} \sigma_{11} & \sigma_{12} \\ \sigma_{21} & \sigma_{22} \end{pmatrix}\begin{pmatrix} -\frac{l}{2} \\ 0 \end{pmatrix} = \begin{pmatrix} F_1^v \\ F_2^v \end{pmatrix} \tag{5}$$

This relations lead to:

$$\sigma_{12} = \sigma_{21} = -\frac{2}{l}F_1^h \tag{6}$$

$$\sigma_{22} = -\frac{2}{l}F_2^h \tag{7}$$

$$F_2^v = F_1^h \tag{8}$$

$$\sigma_{11} = -\frac{2}{l}F_1^v \tag{9}$$

In order to simplify the model, we replace the normal stresses on the boundary CD by three forces $F_1$, $F_2$ and $F_3$ concentrated at the points C, M and D, respectively (Fig. 15b). The asymmetry of the applied forces implies that $F_1$, $F_2$ and $F_3$ are different in magnitude. Nevertheless, we assume a linear variation of the forces along the line CD, that is,

$$F_1 - F_2 = F_2 - F_3 \tag{10}$$

Equilibrium requires

$$\Sigma F_x = F + \tau l - \tau' l\, 0 \tag{11}$$

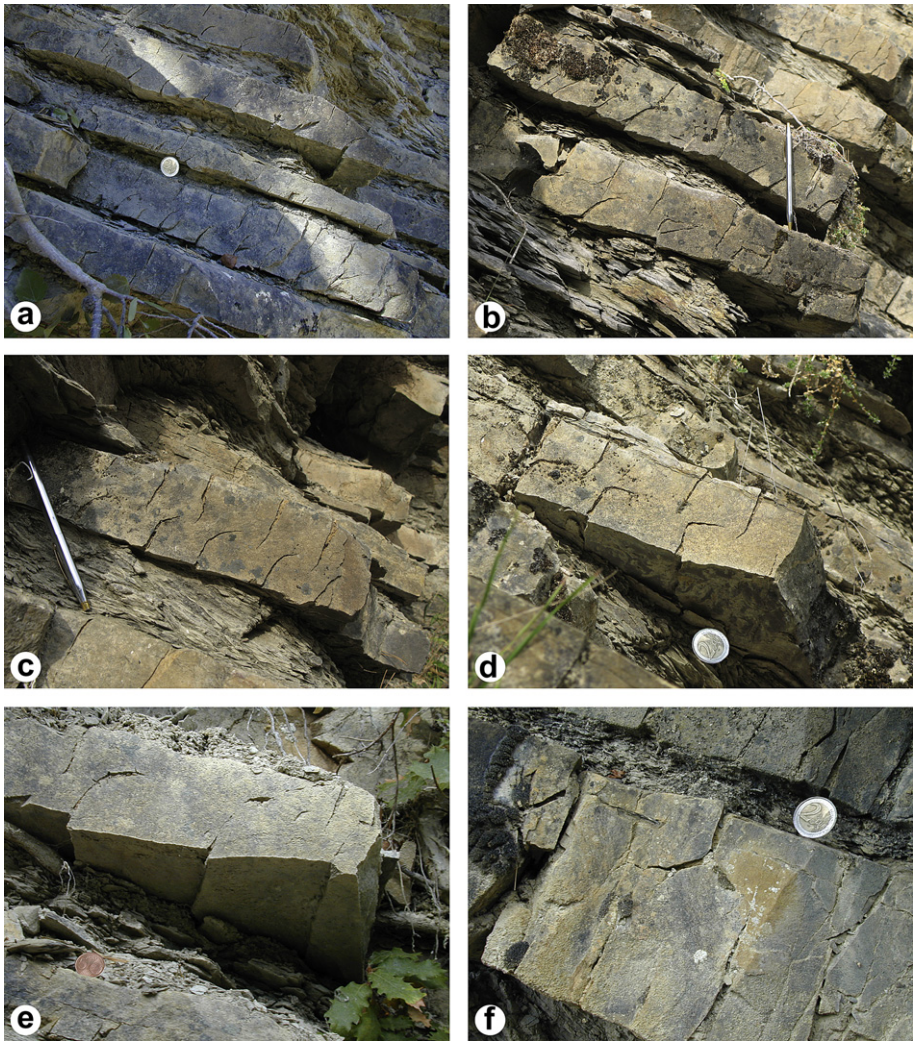


**Fig. 12.** Small dolomite veins developed inside the competent layers. (a, b) General aspect of the veins. (c, d) Detail showing the different morphology of the bottom and top vein sets. (e) Saw-tooth structure at the base of a competent layer. (f) Curved vein developed near the top of a competent layer; note the rotation of the hanging wall. North of Aragüés del Puerto. North to the right.

$$\Sigma F_y = F_1 + F_2 + F_3 + \sigma l = 0 \tag{12}$$

$$\Sigma M_A = \tau' lh + F_2 \frac{l}{2} + F_3 l + \sigma \frac{l^2}{2} = 0 \tag{13}$$

where $M_A$ are the moments about point A. The fourth term of Eq. (13) corresponds to the moment of the distributed force associated with the normal stress $\sigma$. Eqs. (10)–(13) form a system of linear equations that enables all the forces operating on the considered rock element to be obtained.

$$F_1 = -\frac{1}{3}\sigma l + \tau' h \tag{14}$$

$$F_2 = -\frac{1}{3}\sigma l \tag{15}$$

$$F_3 = -\frac{1}{3}\sigma l - \tau' h \tag{16}$$

$$\tau' = \tau + \frac{F}{l} \tag{17}$$

Addition of the forces that operate on a surface element in the $\hat{\mathbf{e}}_1$ direction through the point $C$ gives (Fig. 15c):

$$\mathbf{F}^h = \frac{\tau' l}{3}\hat{\mathbf{e}}_1 - (F_3 + F_1)\hat{\mathbf{e}}_2 \tag{18}$$

$F_3 + F_1$ includes the forces on $C$ of the two adjacent walls of the fracture. We have associated with the point C the shear force $[(\tau' l)/3]\hat{\mathbf{e}}_1$, which is the third part of the total shear force on CD. Taking into account Eqs. (14), (16) and (17), Eq. (18) acquires the form

$$\mathbf{F}^h = \frac{1}{3}(F + \tau l)\hat{\mathbf{e}}_1 + \frac{2}{3}\sigma l \hat{\mathbf{e}}_2 \tag{19}$$

Taking into account Eqs. (6) and (7), we have:

$$\sigma_{12} = -\frac{2}{3}\left(\frac{F}{l} + \tau\right) \tag{20}$$

$$\sigma_{22} = -\frac{4}{3}\sigma \tag{21}$$

For the calculation of $\mathbf{F}^v$, the remaining question is the determination of $F_1^v$, since, in agreement with Eq. (8), $F_2^v = F_1^h = (1/3)(F + \tau l)$.

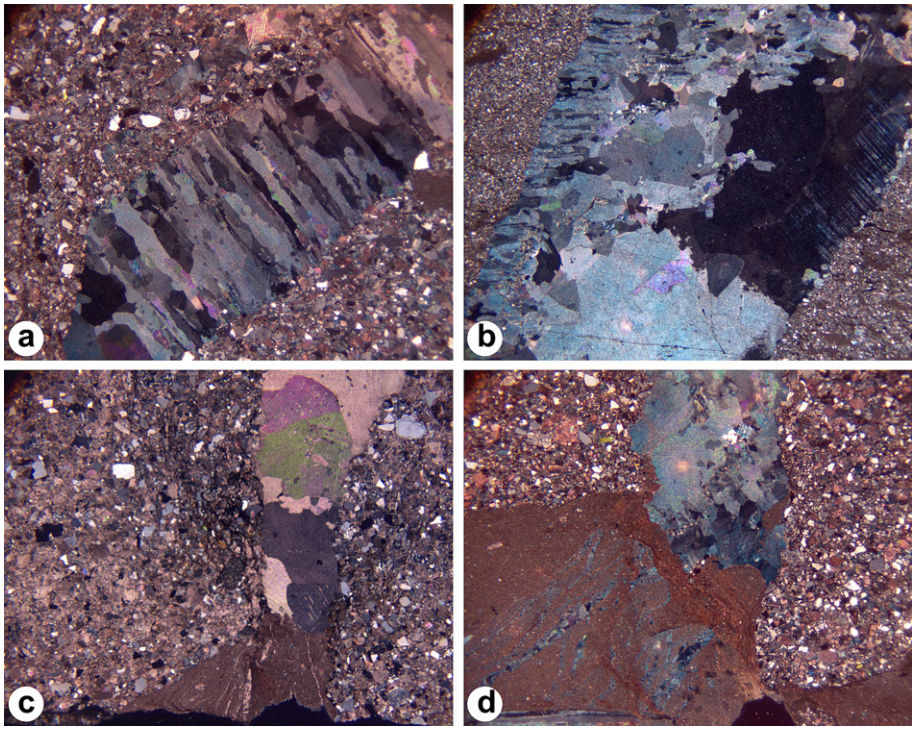


**Fig. 13.** Details of the microscopic aspect of the dolomite veins. (a) Elongate blocky texture. (b) Blocky texture combined with elongate blocky texture near the borders. (c) Blocky texture and mud injection in the mouth of the vein. (d) Blocky texture and deformed step in the base of the bed. Cross polarized light; width of the photographs: 8 mm.

Because the forces along the layer operate in an approximately uniform way, it is expected that the force $F_1^v$ exerted by the left side of the layer on the right side is zero (it is a similar situation to that a train with self-propelling carriages; the interaction between them is null). Hence:

$$F_1^v = 0 \quad \text{and} \quad \sigma_{11} = 0 \tag{22}$$

From the above considerations:

$$\Sigma = \begin{pmatrix} 0 & -b \\ -b & -c \end{pmatrix} \tag{23}$$

where $b = (2/3)((F/l) + \tau)$ and $c = 4\sigma/3$. The eigenvalues of $\Sigma$ are:

$$\sigma_1 = \frac{-c + \sqrt{c^2 + 4b^2}}{2}, \quad (\sigma_1 > 0; \ \text{tensile stress}) \tag{24}$$

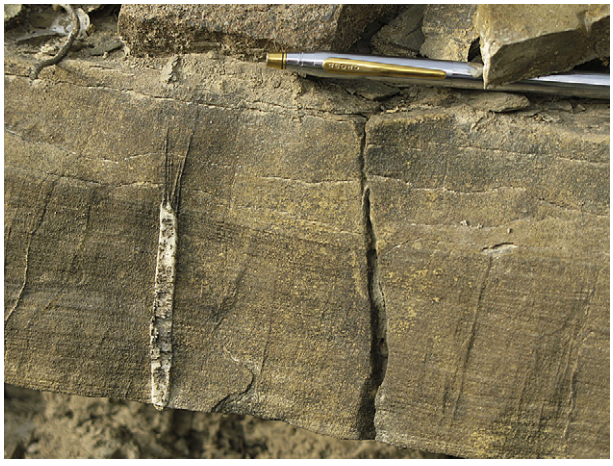

**Fig. 14.** Lithological control on vein development. East of Aragüés del Puerto.

$$\sigma_2 = \frac{-c - \sqrt{c^2 + 4b^2}}{2}, \quad (\sigma_2 < 0; \ \text{compressive stress}) \tag{25}$$

The associated eigenvectors are;

$$v_i = \begin{pmatrix} 1 \\ -\lambda_i/b \end{pmatrix}, \quad (i = 1, 2) \tag{26}$$

Since the fractures open as tension gashes after their formation as small faults, their trends must coincide with the direction of the eigenvector $v_2$ corresponding to the maximum compressive stress $\sigma_2$. The angle that this vector forms with the $\hat{\mathbf{e}}_1$ direction is given by:

$$\tan\varphi = -\frac{\sigma_2}{b} = \frac{1}{2}\left(\frac{c}{b} + \sqrt{\left(\frac{c}{b}\right)^2 + 4}\right), \quad \frac{c}{b} = \frac{2\sigma l}{F + \tau l} \tag{27}$$

This equation shows that the angular inclination of the propagation path of a fracture will be greater the lower the value of the forces ($F$ and $\tau l$) acting in the $\hat{\mathbf{e}}_1$ direction with respect to the force $\sigma l$ acting in the $\hat{\mathbf{e}}_2$ direction (Fig. 16). This obliquity, although it is moderate, alters the geometry of the model analyzed in Fig. 15 in such a way that once the oblique propagation of the fracture is initiated, the force distribution must change and leads probably to a new change in the propagation direction. This change can be analyzed using the finite element method. In this sense, curved fractures with shapes resembling those described here have been described in several non-geological studies that analyze processes as surface cracking during orthogonal machining of glass (Chiu et al., 2001), edge chipping in ceramic materials (Cao, 2001), and chipping in glass plates from line-wedge loading (Chai and Ravichandran, 2007) or from a uniformly applied edge load (Chiu et al., 1998). Analyses conducted by the finite element method in these studies show that stresses acting on a surface of a material can induce cracks in this material that in some cases can show the systematic development of a progressive curvature. The analyses draw conclusions about the structures obtained during abrasion and cutting of different non-

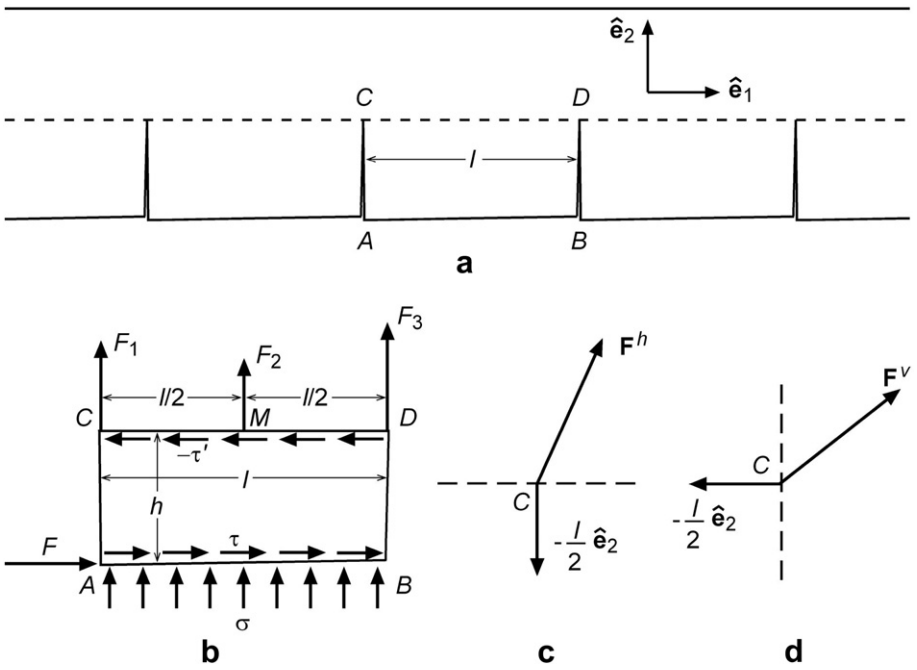


**Fig. 15.** Simple mechanical model to explain the development of the veins. (a) General scheme previous to the development of the widening and curving of the veins. (b) Forces acting on an element ABCD between two adjacent fractures. (c) Resultant force on a surface element in the $\hat{\mathbf{e}}_1$ direction and passing though C. (d) Resultant force on a surface element in the $\hat{\mathbf{e}}_2$ direction and passing through C.

geological materials, but the results can be applied to the structures that can be expected during geological deformation by concentration of shear stresses on the surface of brittle materials.

Chai and Ravichandran (2007) used the finite element method to analyze the fracture patterns obtained for top-surface spalling with different indentation angles. The crack is produced by an indenter whose geometry probably resembles the stress concentration on the steps produced in the small faults of the natural examples analyzed here. In the models of Chai and Ravichandran (2007) (see their Fig. 17), the crack originates from the tip of the indenter and curves progressively. In the models, two sectors can be distinguished in the fracture. The initial part is a stable fracture that develops progressively as the load is applied. In a second stage unstable fracture takes over and the crack deviates towards the specimen surface, producing spalling. It is probable that this unstable part of the fracture is inhibited in the natural cases studied by the stresses acting perpendicular to the bedding planes. The fact that the conditions of the modelling give rise to characteristic shape

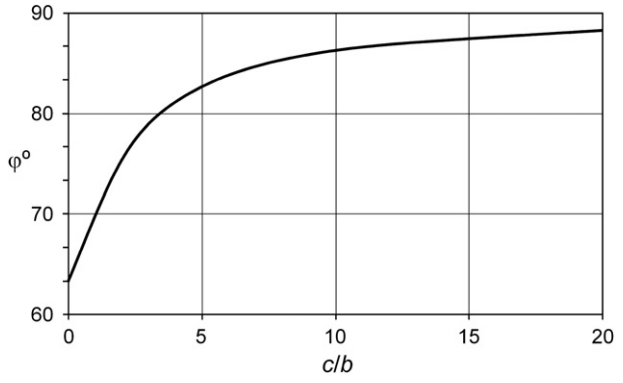


**Fig. 16.** Variation of the angular inclination $\phi$ of the maximum compressive stress direction at point C of Fig. 15 as a function of the parameter $c/b$.

parameters of the fractures can explain the similar morphologies of adjoining veins found in our outcrops in many cases.

## 5. Conclusions

Two generations of folds ($F_1$ and $F_2$) at the outcrop scale developed in the Eocene turbidites (arenites and shales) of the central part of South Pyrenean zone. $F_1$ folds are the most common and represent the second generation of structures at the regional scale. They are close folds, verge towards the foreland of the orogen and exhibit an associated cleavage $S_1$. Geometry of the folded surface profiles mainly ranges between the chevron and parabolic shape. Class 1C folds are dominant in the competent beds. Kinematics of the individual folded competent layers involves a variable initial layer-parallel shortening, tangential longitudinal strain, small or null flexural flow, and superposed small homogeneous deformation close to a simple shear with a shear direction towards the foreland and plunging between 17° and 28°. Flexural slip is an important mechanism when the whole multilayer is considered.

Dolomite veins, formed during the development of $F_1$ folds, are common in competent beds. Usually, the veins show a wedge-like form with a progressively thickening towards the boundary of the layer. A typical array of veins consists of a curved bottom set with the concavity downwards that alternates with a top set with straight or low curvature veins. Mainly in the base of the bed, the displacements involved in the vein development gave rise frequently to steps by which the bedding plane steps up in the direction towards the hinge zone of the adjacent anticline, with a structural pattern that has been named ‘saw-tooth structure’.

Favoured by an initial high fluid pressure, the veins were initiated as small faults conjugated with bedding faults due to flexural slip folding. These small faults gave rise to steps. With the progress of folding, the angle between the direction of the main compressive stress due to the adjacent incompetent material and the bedding increased. On the other hand, the steps hampered the operation of the flexural slip mechanism, and a stress concentration took place

on them. Then, opening and propagation of the fractures as tension gashes were produced and they became veins. The analysis of the forces acting in the vein tip shows that the angle between the maximum compressive stress direction and the bed decreases with the increase of the ratio between the value of the forces operating in a tangential direction of the bed and those operating perpendicularly to the bed. The obliquity between this main direction and the bed explains the change in the propagation direction of the veins, whose curved form can be shown using finite element methods.

## Acknowledgements

The present work was supported by Spanish CGL2008-03786/BTE and CGL2011-23628 projects funded by Ministerio de Ciencia e Innovación y and Fondo Europeo de Desarrollo Regional (FEDER) and the project 'Topo-Iberia' (CSD2006-0041) of the Spanish CONSOLIDER-INGENIO 2010 Program. The authors are grateful to Deepak C. Srivastava and Tom Benkinsop for many valuable suggestions that notably improved the manuscript.

## References

Aller, J., Bobillo-Ares, N.C., Bastida, F., Lisle, R.J., Menéndez, C.O., 2010. Kinematic analysis of asymmetric folds in competent layers using mathematical modeling. Journal of Structural Geology 32, 1170–1184.

Bastida, F., Aller, J., Bobillo-Ares, N.C., Toimil, N.C., 2005. Fold geometry: a basis for their kinematical analysis. Earth-science Reviews 70, 129–164.

Bobillo-Ares, N.C., Toimil, N.C., Aller, J., Bastida, F., 2004. 'Fold modeler': a tool for the geometrical and kinematical analysis of folds. Computer & Geosciences 30, 147–159.

Bobillo-Ares, N.C., Aller, J., Bastida, F., Lisle, R.J., Toimil, N.C., 2006. The problem of area change in tangential longitudinal strain folding. Journal of Structural Geology 28, 1835–1848.

Caja, M.A., Marfil, R., García, D., Remacha, E., Morad, S., Mansurbeg, H., Amorosi, A., Martínez-Calvo, C., Lahoz-Beltrá, R., 2010. Provenance of siliciclastic and hybrid turbiditic arenites of the Eocene Hecho group, Spanish Pyrenees: implications for the tectonic evolution of a foreland basin. Basin Research 22, 157–180.

Cao, Y., 2001. Failure analysis of exit edges in ceramic machining using finite element analysis. Engineering Failure Analysis 8, 325–338.

Chai, H., Ravichandran, G., 2007. On the mechanics of surface and side-wall chipping from line-wedge indentation. International Journal of Fracture 148, 221–231+.

Chiu, W.C., Thouless, M.D., Endres, W.J., 1998. An analysis of chipping in brittle materials. International Journal of Fracture 90, 287–298.

Chiu, W.C., Endres, W.J., Thouless, M.D., 2001. An analysis of surface during orthogonal machining of glass. Machining Science and Technology 5, 195–215.

Gil, A., Simón, J.L., Pueyo, O., Millán, H., Pocoví, A., Andrés, J.A., Arantegui, A., Arlegui, L.E., Arranz, E., Liesa, C.L., Artieda, A., Corella, J.P., Edo, V., Galindo, G., Maestro, A., Sánchez, E., Rico, M.T., Simón, M., Tyrrell, J., 2006. Desarrollo simultáneo de pliegues, esquistosidad y cabalgamientos en el Eoceno inferior de Isaba (Valle del Roncal, Pirineo Navarro). Geogaceta 40, 31–34.

Hudeleston, P.J., 1973. Fold morphology and some geometrical implications of theories of fold development. Tectonophysics 16, 1–46.

Mansurbeg, H., Caja, M.A., Morad, S., Remacha, E., García, D., Martín-Crespo, T., El-Ghali, M.A.C., Nystuen, J.P., 2009. Diagenetic evolution and porosity destruction of turbiditic hybrid arenites and siliciclastic sandstones of foreland basins: evidence from the Eocene Hecho group, Pyrenees, Spain. Journal of Sedimentary Research 79, 711–735.

Mutti, E., Luerbacher, H.P., Ferrer, J., Rosell, J., 1972. Schema stratigrafico e lineamenti di facies del Paleogene marino della zona centrale sudpirenaica tra Tremp (Catalogna) e Pamplona (Navarra). Memorie Della Società Geologica Italiana 11, 391–416.

Pettijohn, F.J., Potter, P.E., Siever, R., 1972. Sand and Sandstone. Harper and Row, New York.

Ramsay, J.G., 1974. Development of chevron folds. Bulletin of the Geological Society of America 85, 1741–1754.

Teixell, A., 1996. The Ansó transect of the southern Pyrenees: basement and cover thrust geometries. Journal of the Geological Society 153, 301–310.

Teixell, A., García-Sansegundo, J., 1995. Estructura del sector central de la Cuenca de Jaca (Pirineos meridinales). Revista de la Sociedad Geológica de España 8, 215–228.

Zuffa, G.G., 1980. Hybrid arenites: their composition and classification. Journal of Sedimentary Petrology 50, 21–29.